Self-Organization of 2,5-Di-*n*-Alkoxy-1,4-benzoquinones in the Solid State: Molecular Recognition Involving Intermolecular Dipole–Dipole, Weak C–H···O=C Hydrogen Bond and van der Waals Interactions

Erik M. D. Keegstra, Valentijn van der Mieden, Jan W. Zwikker, and Leonardus W. Jenneskens*

Debye Institute, Department of Physical Organic Chemistry, Utrecht University, Padualaan 8, 3584 CH Utrecht, The Netherlands

Arie Schouten, Huub Kooijman, Nora Veldman, and Anthony L. Spek

Bijvoet Center for Biomolecular Research, Crystal and Structural Chemistry, Utrecht University, Padualaan 8, 3584 CH Utrecht, The Netherlands

Received November 6, 1995. Revised Manuscript Received January 30, 1996[⊗]

In the solid state 2,5-di-*n*-alkoxy-1,4-benzoquinones **1(*n*)** organize into a two-dimensional layered structure with columnarly stacked 1,4-benzoquinone moieties along the *a* and *b* axis leading to improved intermolecular π-overlap. An interplay between intermolecular merocyanine-type dipole–dipole interactions, directional weak C–H···O hydrogen bond interactions and nondirectional van der Waals interactions is responsible for this packing motif. DSC of **1(*n*)** shows that for *n* = 3–19 pronounced solid–solid phase transitions are discernible. Concomitant with alkoxy chain length odd–even effects are observed. Linear relationships are found between enthalpy and entropy changes, respectively, at distinct phase transitions for **1(*n*)** with *n* ≥ 9 (*n* = odd) and *n* ≥ 10 (*n* = even) indicative for identical packing motifs in both series, respectively. Picnometry reveals that the densities of **1(*n*)** with *n* = odd are higher than those for *n* = even. As shown by single-crystal X-ray structure analyses (**1(3)**, **1(9)**, and **1(10)**) and wide-angle X-ray diffraction (WAXD, **1(*n*)**, 9 ≤ *n* ≤ 19), this can be attributed to improved end-group packing of the alkoxy chains in the odd series.

Introduction

In the design of electroactive materials from relatively simple organics, besides molecular properties, intermolecular self-organization is in numerous cases an additional prerequisite.[1] Although crystal engineering, i.e., formation of a solid-state structure by molecular recognition, allows the preparation of organic solids for application in material science,[2,3] the prediction and design remains a challenging problem considering the number of possible packing motifs available.[4–11]

One of our objectives is to develop one-component molecular systems which exhibit charge-transport properties due to a *face-to-face* stacking of planar electroactive components. 1,4-Benzoquinone derivatives were chosen since they possess multistage redox properties of technological potential[12–17] and biological importance.[18,19] Although in the solid state 1,4-benzoquinones usually give planar sheets due to intermolecular lateral H···O=C hydrogen bond interactions, the intersheet organization required for favorable intermolecular π-overlap is generally thwarted.[20] Recently, we have shown that in the case of methoxy-1,4-benzoquinone the intersheet organization is controlled by intermolecular dipole–dipole interactions and directional weak C–H···O hydrogen bonds leading to a graphite-like packing motif.[21] In a subsequent investigation solid-state packing motifs of tetra-*n*-alkoxy-1,4-benzoquinones were analyzed; due to close packing of the alkoxy chains intersheet organization was considerably improved.[22]

[⊗] Abstract published in *Advance ACS Abstracts,* March 15, 1996.
(1) Lindsey, J. S. *New J. Chem.* **1991,** *15,* 153.
(2) Lehn, J.-M. *Angew. Chem., Int. Ed. Engl.* **1990,** *29,* 1304.
(3) Desiraju, G. R. *Crystal Engineering: The Design of Organic Solids*; Elsevier: New York, 1989; p 160 and references therein.
(4) Zerkowski, J. A.; Seto, C. T.; Wierda, D. A.; Whitesides, G. M. *J. Am. Chem. Soc.* **1990,** *112,* 9025.
(5) Baxter, P.; Lehn, J.-M.; DeCain, A.; Fischer, J. *Angew. Chem., Int. Ed. Engl.* **1993,** *32,* 69.
(6) Pfeil, A.; Lehn, J.-M. *J. Chem. Soc., Chem. Commun.* **1992,** 838.
(7) Garnier, F.; Yassar, A.; Hajlaoui, R.; Horowitz, G.; Deloffre, F.; Servet, B.; Ries, S.; Alnot, P. *J. Am. Chem. Soc.* **1993,** *115,* 8716.
(8) Dhindsa, A. S.; Song, Y.-P.; Badyal, J. P.; Bryce, M. R.; Lvov, Y. M.; Petty, M.C.; Yarkwood, J. *Chem. Mater.* **1992,** *4,* 724.
(9) Marks, T. J. *Angew. Chem., Int. Ed. Engl.* **1990,** *29,* 857.
(10) Crane, J. D.; Sauvage, J.-P. *New J. Chem.* **1992,** *16,* 649.
(11) Pregel, M. J.; Jullien, L.; Lehn, J.-M. *Angew. Chem., Int. Ed. Engl.* **1992,** *31,* 1637.

(12) Chambers, J. Q., Patai, S., Eds. *The Chemistry of the Quinonoid Compounds*; John Wiley & Sons: London, 1974; p 737.
(13) Hünig, S. *Pure Appl. Chem.* **1990,** *62,* 395.
(14) Takazuko, K.; Suzuki, T.; Akiyama, K.; Ikegami, Y.; Fukazawa, Y. *J. Am. Chem. Soc.* **1991,** *113,* 4576 and references therein.
(15) Fabian, J.; Zahradnik, R. *Angew. Chem.* **1989,** *101,* 693.
(16) Schmidt, H.-W. *Angew. Chem. Adv. Mater.* **1989,** *101,* 964.
(17) Meyer, T. J. *Acc. Chem. Res.* **1989,** *101,* 163 and references therein.
(18) Deisenhofer, J.; Epp, O.; Miki, K.; Huber, R.; Michel, H. *J. Mol. Biol.* **1984,** *180,* 385.
(19) Allen, J. P.; Feher, G.; Yeates, T. O.; Komiya, H.; Rees, D. C. *Proc. Natl. Acad. Sci. U.S.A.* **1987,** *84,* 5730.
(20) Bernstein, J.; Cohen, M. D., Leiserowitz, L., Patai, S., Eds. *The Chemistry of the Quinonoid Compounds*; John Wiley & Sons: London, 1974; pp 37–110.
(21) Keegstra, E. M. D.; Spek, A. L.; Zwikker, J. W.; Jenneskens, L. W. *J. Chem. Soc., Chem. Commun.* **1994,** 1633.
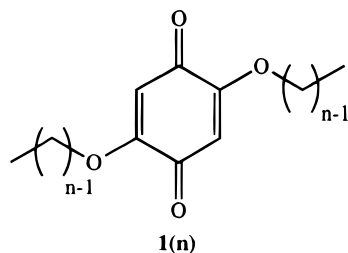
Figure 1. Compounds **1(*n*)**.

Their self-organization is mainly based on lateral C−H···O hydrogen bonds, reduction of unfavorable dipole−dipole and van der Waals interactions (close packing principle of the *n*-alkoxy chains). However with increasing length of the *n*-alkoxy chains, the efficacy of the intersheet packing of the 1,4-benzoquinone moieties is partly destroyed due to the efficient packing of the four alkoxy chains. Therefore, we were prompted to study the related 2,5-substituted 1,4-benzoquinones. In a preliminary investigation we have shown that the 1,4-benzoquinone moieties of 2,5-di-*n*-decoxy-1,4-benzo-quinone assemble efficiently cofacially in the solid state and that, indeed, rapid charge migration takes place when using temperature-dependent pulse radiolysis microwave conductivity measurements (TRMC).[23] Because *n*-alkoxy chain length can be readily varied and interactions between these chains can lead to a reduction of the interplanar distance between adjacent π-moieties,[24] a series of 2,5-di-*n*-alkoxy-1,4-benzoquinones (**1(*n*)**; *n* = number of carbon atoms per alkoxy chain) with *n* = 1−19 has been synthesized (Figure 1). Their solid-state self-organization with respect to *n*-alkoxy chain length is the subject of this article.

Experimental Section

Analytical Techniques. NMR spectra were recorded on a Bruker AC 300 MHz spectrometer (^{1}H 300 MHz; ^{13}C 75 MHz) using the solvent as internal standard (CDCl$_3$ ^{1}H, δ 7.26 ppm; ^{13}C, δ 77.00 ppm). Diffuse reflection infrared FT spectra were recorded on a Mattson Galaxy Series FTIR 5000 spectrophotometer; the samples were diluted with optical pure KBr.

Cyclic Voltammetry. Cyclic voltammograms of **1(*n*)** with *n* = 1, 2, 3, and 4 were recorded in acetonitrile containing *n*-Bu$_4$PF$_6$ (10^{-1} M) as electrolyte, at voltage sweep rates of 50, 100, and 200 mV s^{-1}. The following three-electrode arrangement was used; Pt as working and counter electrodes together with a separated Ag/AgCl reference electrode in acetonitrile, containing *n*-Bu$_4$PF$_6$ (10^{-1} M), connected via a salt bridge. Maximum compensation for *iR* drop was achieved by utilizing a PAR 273 potentiostat. Reduction potentials are reported against the $E_{1/2}^{red}$(0/−1) of ferrocene/ferrocinium used as an internal standard.[25]

Differential Scanning Calorimetry. The thermal properties of compounds **1(*n*)** were investigated by DSC (Mettler DSC 12E). The following heating and cooling sequence was applied: Compounds **1(*n*)** were heated from 25 to 10 °C above their melting point and afterward cooled to −10 °C. Subsequently, they were heated from −10 °C again to 10 °C

above their melting point and finally cooled down to −10 °C (heating rate 2 °C/min and cooling rate 5 °C/min). Unless indicated otherwise, the onsets of the DSC peaks are taken as transition temperature. The enthalpy values are calibrated versus an indium standard.

Picnometry. Densities of compounds **1(*n*)** with *n* is 2−16 and 18 were determined in quadruplicate at 25.3 ± 0.1 °C using picnometry (picnometer volume 10 mL, solvent *n*-decane).[26] All weight measurements were performed on an analytical balance (accuracy ±0.1 mg).

Powder Wide-Angle X-ray Diffraction (WAXD). Powder wide-angle X-ray diffraction patterns were recorded at room temperature using a Delft Instruments Guinier Johansson FR552 camera at a wavelength of 1.5405 Å.

Single-Crystal X-ray Determination of 1(3), 1(9), and 1(10). Crystals suitable for X-ray structure determination were glued to the top of a Lindeman-glass capillary and transferred to an Enraf-Nonius CAD4-T diffractometer on a rotating anode [**1(3)** and **1(10)**] or to an Enraf-Nonius CAD4-F sealed tube diffractometer [**1(9)**]. Accurate unit-cell parameters and an orientation matrix were determined by least-squares refinement of the setting angles of a set of well-centered reflections (SET4,[27] in the ranges 8.52° < θ < 16.86° [25 reflections], 12.97° < θ < 26.45° [22 reflections] and 8.28° < θ < 15.45°, [23 reflections] for **1(3)**, **1(9)**, and **1(10)**, respectively. The unit-cell parameters were checked for the presence of higher lattice symmetry.[28] Crystal data and details on data collection are presented in Table 1. Data were corrected for *Lp* effects and for the linear decay of three periodically measured reference reflections during X-ray exposure time. For compound **1(10)** the standard deviations of the intensities as obtained by counting statistics were increased according to an analysis of the excess variance of the reference reflections: $\sigma^2(I) = \sigma_{cs}^2(I) + (0.03I)^2$.[29] An empirical absorption correction (DIFABS[30]) was applied for compound **1(9)**. All structures were solved by automatic direct methods using SIR-92,[31] for compound **1(3)** and SHELXS86[32] for compounds **1(9)** and **1(10)**. Refinement on *F* was carried out by full-matrix least-squares techniques (SHELXS76[33] for compounds **1(3)** and **1(10)**). Compound **1(9)** was refined on F^2 using full-matrix least-squares techniques (SHELXS93[34]); no observance criterium was applied during refinement. Hydrogen atoms of **1(3)** were located on a difference Fourier map and subsequently included in the refinement. Hydrogen atoms of the other compounds were included in the refinement on calculated positions riding in their carrier atoms. All non-hydrogen atoms were refined with anisotropic thermal parameters. The hydrogen atoms of **1(3)** were refined with individual isotropic thermal parameters. The hydrogen atoms of **1(9)** were included in the refinement with a fixed isotropic thermal parameter related to the value of the equivalent isotropic thermal parameter of their carrier atoms by a factor of 1.5 for the methyl hydrogen atoms and 1.2 for the other hydrogen atoms. For compound **1(10)** the overall isotropic thermal parameter for the hydrogen atoms attached to C(12) and C(13) refined to a value of 0.163(10) Å^2; the overall isotropic thermal parameter for the other hydrogen atoms refined to a value of 0.069(3) Å^2. Positional parameters of **1(3)**, **1(9)**, and **1(10)** are listed in the supporting information. Neutral atom scattering factors and anomalous dispersion corrections were taken from the International Tables for

(22) Keegstra, E. M. D.; Huisman, B.-H.; Paardekooper, E. M.; Hoogesteger, F. J.; Zwikker, J. W.; Jenneskens, L. W.; Kooijman, H.; Schouten, A.; Veldman, N.; Spek, A. L. *J. Chem. Soc., Perkin Trans 2* **1996**, 229.

(23) Keegstra, E. M. D.; Schouten, P. G.; Schouten, A.; Kooijman, H.; Spek, A. L.; De Haas, M. P.; Zwikker, J. W.; Warman, J. M.; Jenneskens, L. W. *Recl. Trav. Chim. Pays-Bas* **1993**, *112*, 423.

(24) Shi, Z.; Enoki, T.; Imaeda, K.; Seki, K.; Wu, P.; Inokuchi, H.; Satio, G. *J. Phys. Chem.* **1988**, *92*, 5044.

(25) Gagné, R. R.; Koval, C. A.; Lisenky, G. C. *Inorg. Chem.* **1980**, *19*, 2855.

(26) West, A. R. *Basic Solid State Chemistry*; John Wiley & Sons: New York, 1988.

(27) de Boer, J. L.; Duisenberg, A. J. M. *Acta Crystallogr.* **1984**, *A40*, 410.

(28) Spek, A. L. *J. Appl. Crystallogr.* **1988**, *21*, 578.

(29) McCandlish, L. E.; Stout, G. H.; Andrews, L. C. *Acta Crystallogr.* **1975**, *A31*, 245.

(30) Walker, N.; Stuart, D. *Acta Crystallogr.* **1983**, *A39*, 158.

(31) Sheldrick, G. M. *SHELXS86 Program for crystal structure determination,* University of Göttingen, Germany, 1986.

(32) Altomare, A.; Cascarano, G.; Giacovazzo, C.; Guagliardi, A. *J. Appl. Cryst.* **1993**, *26*, 343.

(33) Sheldrick, G. M. *SHELXS76 Program for crystal structure determination,* University of Cambridge, England, 1976.

(34) Sheldrick, G. M. *SHELXS93 Program for crystal structure refinement,* University of Göttingen, Germany, 1993.

Table 1. Crystallographic Data for 1(3), 1(9), and 1(10)

	1(3)	1(9)	1(10)
Crystal Data			
formula	$C_{12}H_{16}O_4$	$C_{24}H_{40}O_4$	$C_{26}H_{44}O_4$
molecular weight	224.26	392.58	420.63
crystal system	triclinic	triclinic	triclinic
space group	$P\bar{1}$ (No. 2)	$P\bar{1}$ (No. 2)	$P\bar{1}$ (No. 2)
a, Å	4.2258(3)	4.1996(5)	4.2118(3)
b, Å	5.1429(4)	5.3552(2)	5.3337(5)
c, Å	13.3801(11)	26.044(2)	28.8117(19)
α, deg	78.947(7)	87.489(5)	91.826(6)
β, deg	86.409(6)	86.677(9)	92.775(5)
γ, deg	89.042(6)	86.980(7)	92.992(7)
V, Å^3	284.83(4)	583.44(9)	645.22(9)
D_{calc}, g/cm^3	1.307	1.117	1.082
Z	1	1	1
$F(000)$	120	216	232
μ, cm^{-1}	0.9 [Mo Kα]	5.5 [Cu Kα]	0.7 [Mo Kα]
crystal size, mm	0.05 × 0.30 × 1.00	0.1 × 0.4 × 0.6	0.05 × 0.09 × 0.78
Data Collection			
T, K	150	295	298
θ_{min}, θ_{max}, deg	1.6, 27.5	1.7, 75.0	0.7, 27.5
wavelength, Å	0.71073 [Mo Kα, graphite monochr]	1.54185 [Cu Kα, Ni filter]	0.71073 [Mo Kα, graphite monochr]
scan type	$\omega/2\theta$	$\omega/2\theta$	$\omega/2\theta$
$\Delta\omega$, deg	0.91 + 0.35 tan θ	0.72 + 0.14 tan θ	0.80 + 0.35 tan θ
hor, ver aperture, mm	3.88, 4.00	2.94, 6.00	3.00, 4.00
X-ray exposure time, h	12	34	20
linear decay, %	2	1	1
reference reflections	2 $\bar{1}$ $\bar{3}$, 1 $\bar{2}$ $\bar{5}$, 3 $\bar{2}$ $\bar{2}$	$\bar{2}$ 0 5, 0 $\bar{2}$ 8, 0 $\bar{2}$ 2	$\bar{2}$ 2 0, 0 2 7, $\bar{2}$ 1 2
data set	−4:5, −6:6, −17:17	−5:4, −6:6, −32:32	−5:5, −6:6, −37:37
total data	2403	4237	3508
total unique data	1316 [R_{int} = 0.023]	2408 [R_{int} = 0.058]	2938 [R_{int} = 0.032]
obsd data	1053 [$I > 2.5\sigma(I)$]	[no obs crit applied]	1294 [$I > 2.5\sigma(I)$]
DIFABS corr range		0.454, 1.782	
Refinement			
no. of refined params	105	128	141
final R^a	0.041	0.050 [757, $I > 2\sigma(I)$]	0.060
final $wR2^b$		0.138	
final $R_w{}^c$	0.051		0.062
goodness of fit	1.83	0.75	0.48
w^{-1d}	$\sigma^2(F) + 0.000455F^2$	$\sigma^2(F^2) + (0.0786P)^2$	$\sigma^2(F)$
$(\Delta/\sigma)_{av}$, $(\Delta/\sigma)_{max}$	0.028, 0.121	0.000, 0.000	0.023, 0.103
min and max residual density, e Å^{-3}	−0.24, 0.32	−0.21, 0.16	−0.22, 0.20

^{a} $R = \sum ||F_o| - |F_c||/\sum |F_o|$. ^{b} $wR2 = [\sum[w(F_o{}^2 - F_c{}^2)^2]/\sum[w(F_o{}^2)^2]]^{1/2}$. ^{c} $R_w = [\sum[w(||F_o| - |F_c||)^2]/\sum[w(F_o{}^2)]]^{1/2}$. ^{d} $P = (\max(F_o{}^2,0) + 2F_c{}^2)/3$.

Crytallography[35] for compound **1(9)**. For compounds **1(3)** and **1(10)** neutral atom scattering factors were taken from Cromer and Mann;[36] anomalous dispersion corrections from Cromer and Liberman.[37] Geometrical calculations and illustrations were performed with PLATON[38] and PLUTON.[39] All calculations were performed on a DEC5000 cluster.

Materials. 2,5-Dihydroxy-*p*-benzoquinone was purified before use.[22] Boron trifluoride etherate was applied as obtained. The purity of the utilized *n*-alkanols (99%; Aldrich) was checked with capillary gas chromatography after trimethylsilylation of the hydroxyl endgroup.[40] Compounds **1(n)** with *n* = 2−19 were synthesized, according to a modified procedure.[41] Compound **1(1)** could not be prepared by this method and was prepared by etherification of 2,5-dihydroxy-1,4-benzoquinone in a MeOH solution saturated with HCl.[42]

General Procedure for the Synthesis of 2,5-Di-*n*-alkoxy-1,4-benzoquinones (1(n)). A three-necked flask equipped with a reflux condenser was charged with 2,5-

dihydroxy-1,4-benzoquinone (5 g, 36 mmol), the appropriate *n*-alkanol (360 mmol), and boron trifluoride etherate (9 mL, 72 mmol). For *n*-dodecanol and higher homologues THF (50 mL) had to be added to dissolve the *n*-alkanol completely. The homogeneous reaction mixture was heated at 80 °C for 2 h. Crude compounds **1(n)** were obtained from the reaction mixture by crystallization at −20 °C and purified by recrystallization (twice) from THF at −20 °C (1 g/mL). Spectral characterization (^{1}H and ^{13}C NMR and DRIFT spectroscopy) revealed that compounds **1(n)** were pure.

2,5-Dimethoxy-1,4-benzoquinone (1(1)): yield 4.08 g (24.3 mmol, 68%). ^{1}H NMR δ 5.93 (s, 2H); 3.85 (s, 6H) ppm; ^{13}C NMR δ 184.32, 160.93, 105.28, 13.72 ppm. DRIFT ν 3000.6, 2960.2, 2861.4, 1672.6, 1611.3, 1232.9, 1370.4, 1285.1, 1230.6 cm^{-1}.

2,5-Di-*n*-propoxy-1,4-benzoquinone (1(3)): yield 3.42 g (16.8 mmol, 47%). ^{1}H NMR δ 5.77 (s, 2H); 3.83 (t, 4H); 1.82 (m, 4H); 0.97 (t, 6H) ppm. ^{13}C NMR δ 181.78, 158.61, 105.62, 71.00, 21.41, 10.13 ppm. DRIFT ν 2977.7, 2967.6, 2942.5, 2933.4, 1670.2, 1607.0, 1230.0, 1209.2 cm^{-1}.

2,5-Di-*n*-nonoxy-1,4-benzoquinone (1(9)): yield 6.02 g (15.3 mmol, 43%). ^{1}H NMR δ 5.81 (s, 2H); 3.90 (t, 4H); 1.80 (dt, 4H); 1.30 (m, 24H); 0.85 (t, 6H) ppm. ^{13}C NMR δ 181.89, 158.72, 105.68, 69.76, 31.73, 29.31, 29.11, 28.08, 25.70, 22.55, 14.00 ppm. DRIFT ν 2951.7, 2929.5, 2915.1, 2849.5, 1673.0, 1605.1, 1472.0, 1225.6, 1206.3 cm^{-1}.

2,5-Di-*n*-decyloxy-1,4-benzoquinone (1(10)):[41] yield 5.25 g (12.5 mmol, 35%). ^{1}H NMR δ 5.78 (s, 2H); 3.86 (t, 4H); 1.76 (dt, 4H); 1.30 (m, 28H); 0.83 (t, 6H) ppm. ^{13}C NMR δ 181.96, 158.83, 105.78, 69.84, 31.84, 29.47, 29.43, 29.25, 29.18, 28.16,

(35) Wilson, A. J. C. *International Tables for Crystallography*, Volume C, 1992; Kluwer Academic Publishers: Dordrecht, The Netherlands.

(36) Cromer, D. T.; Mann, J. B. *Acta Crystallogr.* **1968**, *A24*, 321.

(37) Cromer, D. T.; Liberman, D. *J. Chem. Phys.* **1970**, *53*, 1891.

(38) Spek, A. L. *Acta Crystallogr.* **1990**, *A46*, C34.

(39) Spek, A. L. *PLUTON Molecular graphics program*, Utrecht University, The Netherlands, 1995.

(40) Sweely, C. C.; Bently, R.; Makita, M.; Wells, W. W. *J. Am. Chem. Soc.* **1963**, *85*, 2497.

(41) Rodriguez-Parada, J. M.; Duran, R.; Wegner, G. *Macromolecules* **1989**, *22*, 2507.

(42) Crosby, A. H.; Lutz, R. E. *J. Am. Chem. Soc.* **1956**, *78*, 1233.

Self-Organization in the Solid State

Chem. Mater., Vol. 8, No. 5, 1996 1095

25.78, 22.64, 14.07 ppm. DRIFT ν 2954.1, 2927.6, 2916.0, 2894.3, 1671.1, 1608.9, 1469.6, 1231.9, 1209.7 cm^{-1}.

2,5-Di-n-dodecyloxy-1,4-benzoquinone (1(12)):[41] yield 8.85 g (18.6 mmol, 52%). ^{1}H NMR δ 5.82 (s, 2H); 3.91 (t, 4H); 1.84 (dt, 4H); 1.30 (m, 36H); 0.87 (t, 6H) ppm. ^{13}C NMR δ 181.97, 158.78, 105.74, 69.82, 31.87, 29.57, 29.49, 29.41, 29.30, 29.17, 28.13, 25.75, 22.64, 14.09 ppm. DRIFT ν 2930.0, 2916.5, 2850.4, 1673.0, 1606.5, 1472.5, 1228.3, 1206.8 cm^{-1}.

Results and Discussion

Influence of 2,5-n-Alkoxy Substitution on the Redox Properties of 1(n). The effect of n-alkoxy substituents on the redox properties of the 1,4-benzoquinone moiety was studied with cyclic voltammetry. Voltammograms of **1(n)** with $n = 1-4$ revealed quasi-reversible behavior for the conversion to the radical anion (0/−1), and irreversible behavior for the radical anion/dianion (−1/−2) conversion.[43] The length of the alkoxy chain has no influence on the value of reduction potentials and the reversibility of the waves. The half-wave reduction potentials $E_{1/2}^{red}(0/-1)$ and $E_{1/2}^{red}(-1/-2)$ are −1.17 and −2.3 V, respectively, against the ferrocene/ferrocinium couple.[25] For the parent compound 1,4-benzoquinone $E_{1/2}^{red}(0/-1)$ and $E_{1/2}^{red}(-1/-2)$ are −0.91 and −2.0 V, respectively. Thus, the electron affinity of quinones **1(n)** decreases ca. 0.3 V compared to 1,4-benzoquinone. This is in line with the expected mero-cyanine-type distortion of the 1,4-benzoquinone skeleton in these 2,5-di-n-alkoxy-1,4-benzoquinones (vide infra).[21,22]

Thermal Analysis. Investigation of the thermal properties of **1(n)** ($n = 1-19$) using DSC provides insight in the dependence of the melting point (T_m) concomitant with alkoxy chain length. The data show a decrease of T_m with increasing n (Figure 2). Distinct solid−solid phase transitions are observed for compounds **1(n)** with $n \geq 3$. In Tables 2 and 3 melting points (T_m), thermotropic solid−solid phase transition temperatures (T_s) and related enthalpy changes (ΔH) taken from the first and second DSC heating runs, respectively, are presented. For convenience, the distinct phases are identified with consecutive Greek characters starting from the *isotropic* liquid phase (eq 1); **m**, **s1**, **s2**, etc., depict the corresponding melting and solid−solid phase transitions, respectively.

$$\text{liquid} \overset{\mathbf{m}}{\longleftarrow} \alpha \overset{\mathbf{s1}}{\longleftarrow} \beta \overset{\mathbf{s2}}{\longleftarrow} \gamma \text{ etc.} \qquad (1)$$
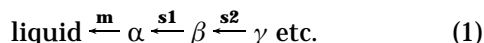
The first solid−solid phase transition (**s1**, $\beta \rightarrow \alpha$) of **1(n)** is the most pronounced one with enthalpy changes that correspond to two-thirds of the enthalpy change at melting. A clear odd−even effect is discernible for 6 $\leq n \leq$ 14 of both T_{s1} and the accompanying enthalpy change ΔH_{s1} (Figure 2). For **1(n)** with n is odd T_{s1} and ΔH_{s1} values are higher. In addition, a pronounced odd−even effect is found for ΔH_m with $n \geq 12$. However, this is not accompanied by a distinct odd-even effect for T_m. To gain more insight into these phenomena, the thermal properties of the odd and even series of **1(n)** were analyzed in detail.

Analysis of Thermal Properties of 1(n) with n = Odd. With the exception of **1(n)** ($n = 1, 3, 7$, and ≥ 15) pristine **1(n)** display two pronounced solid−solid phase transitions in their first DSC heating curve (**s2**, $\gamma \rightarrow \beta$ and
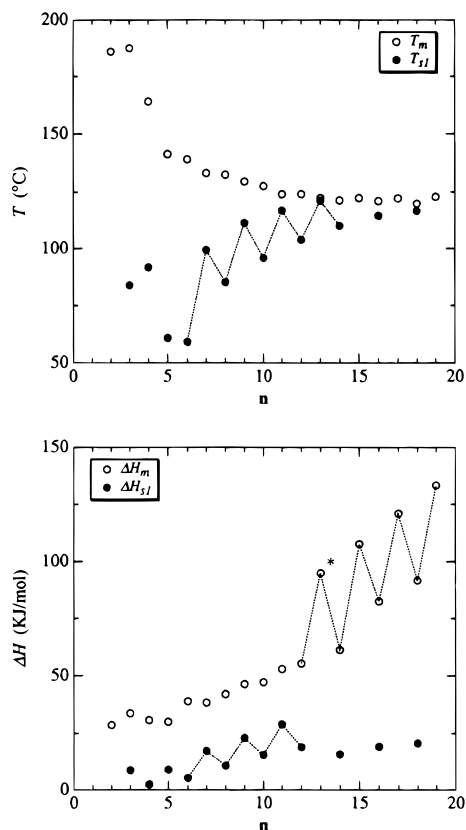

Figure 2. (a, top) Melting point (T_m) and solid−solid phase transition temperature (T_{s1}) dependence from the number of carbon atoms per alkyl chain (n); (b, bottom) Enthalpy changes at T_m and T_{s1}. In the case of $n = 13^*$ the melting and the **s1** solid−solid phase transition coincide.

s1, $\beta \rightarrow \alpha$; Figure 3). Compound **1(1)** decomposes at 190 °C without showing any solid−solid phase transition, while **1(3)** and **1(7)** do not contain the second solid−solid phase transition. For compounds **1(n)** with $n \geq 15$ the first solid−solid phase transition coincides with the melting peak; this is supported by the sudden increase of ΔH_m. Subsequent cooling and heating runs showed the reversibility of the melting and first solid−solid phase transitions. In contrast, the second solid−solid phase transition (**s2**) was either absent or replaced by novel, minor solid−solid phase transitions (Figure 3).

For n-paraffins linear relationships exist between enthalpy as well as entropy changes at distinct phase transitions as a function of alkyl chain length in both the odd and even series.[44,45] According to X-ray analyses these observations can be related to identical packing motifs within both series. For this reason we searched for linear relationships between n and $\Delta\Delta H$ as well as $\Delta\Delta S$ at the different phase transitions (eqs 2 and 3). Indeed, for pristine **1(n)** with $9 \leq n \leq 19$ linear

$$\Delta\Delta H(\mathbf{1(n)}) = \Delta H^\circ + n\Delta H \qquad (2)$$

$$\Delta\Delta S(\mathbf{1(n)}) = \Delta S^\circ + n\Delta S \qquad (3)$$

relationships are found for (i) the total sum of both enthalpy and entropy changes (ΔH_{total} and ΔS_{total}), (ii) the sum of the enthalpy as well as entropy changes at

(43) Heinze, J. *Angew. Chem. Adv. Mater.* **1984**, *96*, 823.

(44) Broadhurst, M. G. *J. Chem. Phys.* **1962**, *36*, 2578.
(45) Broadhurst, M. G. *J. Res. Natl. Bur. Stand., Sect. A* **1962**, *66*, 241 and references therein.

Table 2. Melting Points (T_m), Enthalpy Changes at Melting Points (ΔH_m), Solid–Solid Phase Transition Temperatures (T_s), and Enthalpy Changes at Solid–Solid Phase Transitions (ΔH_s) Observed in the First DSC Heating Run, Densities (d, Picnometry) with the Resulting Molecular Volumes (V_{mol}), Interlayer Spacings ($1/|c^*|$) from the WAXD Patterns of Pristine $1(n)$ and Calculated Molecular Volumes (V_{calc})

$1(n)$	T_m (°C)	ΔH_m (kJ/mol)	T_{s1} (°C)	ΔH_{s1} (kJ/mol)	T_{s2} (°C)	ΔH_{s2} (kJ/mol)	$T_{s3}{}^a$ (°C)	ΔH_{s3} (kJ/mol)	d (g/cm³)	V_{mol} (Å³)	$1/|c^*|$ (Å)	$V_{calc}{}^b$ (Å³)
1	190^c										8.30	
2	186.3	29.0							1.223	266.4	12.44	
3	187.6	33.6	83.6	8.8					1.273	292.5	13.28	
4	164.3	31.5	90.8	2.3	54.8	4.8			1.175	356.6	15.91	
5	142.0	38.1	61.5	9.0	50.8	1.4			1.165	399.6	17.84	
6	139.1	39.5	61.3	4.7					1.111	461.0	20.56	
7	133.6	40.7	99.4	17.6					1.125	496.7	22.07	
8	132.6	43.0	85.0	9.4					1.092	554.3	25.22	
9	129.5	47.1	110.6	24.2	79.4	8.0			1.113	585.7	25.90	581.7
10	127.7	49.6	95.0	15.2					1.072	651.6	29.92	671.2
11	124.0	52.1	116.8	28.4	94.2	12.9			1.096	679.8	29.92	672.0
12	124.0	56.7	104.1	19.4	73.1	8.5			1.078	734.4	33.00	740.3
13	122.4	94.9^d	121.2		107.1	17.4			1.085	772.6	34.17	767.4
14	121.3	69.8	111.4	21.4	82.3	14.8			1.057	837.1	37.24	835.4
15	122.3	107.7			112.7	21.7			1.072	869.7	38.65	868.0
16	121.0	83.0	115.8	19.0	97.7	14.1	84.5	6.7	1.052	929.7	41.06	921.1
17	122.3	120.9			114.9	25.9					42.70	959.0
18	120.0	115.5^d	117.0		94.6	17.2	79.1	4.6	1.046	1024.1	45.65	1024.1
19	123.0	134.0			117.9	30.3					46.70	1048.8

^{a} Transition temperature at the top of the DSC peak. ^{b} $V = |a||b| \cos \gamma/|c^*|$. ^{c} Decomposition. ^{d} $\Delta H_{(m+s1)}$, overlapping transitions.

Table 3. Melting Points (T_m), Enthalpy Changes at Melting Points (ΔH_m), Solid–Solid Phase Transition Temperatures (T_s), and Enthalpy Changes at Solid–Solid Phase Transitions (ΔH_s) Observed in the Second DSC Heating Run, and Interlayer Spacings ($1/|c^*|$) from the WAXD Patterns of $1(n)$ after Annealing Recorded at Room Temperature

$1(n)$	T_m (°C)	ΔH_m (kJ/mol)	T_{s1} (°C)	ΔH_{s1} (kJ/mol)	T_{s2} (°C)	ΔH_{s2} (kJ/mol)	$T_{s3}{}^a$ (°C)	ΔH_{s3} (kJ/mol)	T_{s4} (°C)	ΔH_{s4} (kJ/mol)	$1/|c^*|$ (Å)
2	186.1	28.7									12.44
3	187.6	33.6	83.8	8.6							13.28
4	164.1	30.8	91.3	2.3	55.1	4.7					15.91
5	141.4	36.5	60.5	9.0							17.84
6	138.9	38.9	59.1	5.3							20.56
7	133.0	38.4	99.3	17.3	2.6	3.6					22.07
8	132.3	41.9	85.2	10.8							25.22
9	129.4	46.3	109.3	23.0	35.5	7.3					25.77
10	127.6	47.1	94.6	15.4	−0.8	6.0					29.92
11	123.9	53.0	116.8	28.9	62.7	5.0	45.4	5.4			30.01
12	123.9	55.3	103.8	19.1	46.2	2.1					33.63
13	122.3	61.1	121.2	33.8	86.9	5.7	60.1	1.7	18.9	2.4	34.33
14	121.3	61.3	110.1	15.8^b							37.83
15	122.2	107.7			107.0	7.1	101.0	3.7			38.95
16	121.0	82.5	114.6	19.1	98.0	5.4	87.1	1.3			41.71
17	122.1	120.9			110.4	13.0					43.27
18	119.9	91.6	116.7	20.6	100.6	13.4					46.83
19	122.7	133.3			112.3	16.16					47.46

^{a} Transition temperature at the top of the DSC peak. ^{b} Additional solid–solid phase transition of $1(14)$ at 119.0 °C (7.2 kJ/mol).

melting and the first solid–solid phase transition ($\Delta H_{(m+s1)}$ and $\Delta S_{(m+s1)}$), and (iii) the enthalpy and entropy changes at second phase transition (**s2**, ΔH_{s2} and ΔS_{s2}, see Figure 3 and Table 4).

This indicates that odd compounds $1(n)$ possess identical alkoxy chain packing motifs within the distinct phases α, β, and γ. The slopes (ΔH and ΔS, respectively) of the corresponding lines together with their intercepts (ΔH° and ΔS°, respectively) are given in Table 4.

Analogous relations are found for $1(n)$ with $9 \leq n \leq 19$ from the results of the second DSC heating runs: (i) the total sum of both enthalpy and entropy changes (ΔH_{total} and ΔS_{total}) and (ii) the sum of enthalpy and entropy changes at melting and the first solid–solid phase transition ($\Delta H_{(m+s1)}$ and $\Delta S_{(m+s1)}$, see Figure 3 and Table 4).

The slopes $\Delta H_{(m+s1)}$ (6.42 kJ mol^{-1}) and $\Delta S_{(m+s1)}$ (16.19 J K^{-1} mol^{-1}), and the intercepts $\Delta H_{(m+s1)}^\circ$ (11.5 kJ mol^{-1}) and $\Delta S_{(m+s1)}^\circ$ (29.6 J K^{-1} mol^{-1}) correspond to those obtained from the first DSC heating curve. This

substantiates the thermal reversibility of the α and β phase for the higher homologues. However, the second phase transition (**s2**, $\gamma \rightarrow \beta$) is not thermally reversible. New minor solid–solid phase transitions are observed (vide infra, WAXD analysis and supporting information).

Upon melting pristine $1(n)$, a total enthalpic and entropic change per CH$_2$ group of 4.33 kJ mol^{-1} ($\Delta H_{total}/2$) and 10.78 J K^{-1} mol^{-1} ($\Delta S_{total}/2$), respectively, is found (Table 4). These values are in satisfactory agreement with the enthalpy (4.07 kJ mol^{-1}) and entropy (10.7 J K^{-1} mol^{-1}) changes per CH$_2$ group found for n-parafins with an even number of carbon atoms in going from a triclinic packing motif to the isotropic liquid (see Table 5). This indicates that the alkoxy chains of pristine $1(n)$ with $9 \leq n \leq 19$ possess a triclinic alkyl chain packing (vide infra, single-crystal X-ray analysis).

Insight in the change of thermal mobility of the alkoxy chains upon going through a phase transition is obtained from a comparison of the increments ΔH and ΔS with ΔH_{total} and ΔS_{total}, respectively. At the phase

Self-Organization in the Solid State

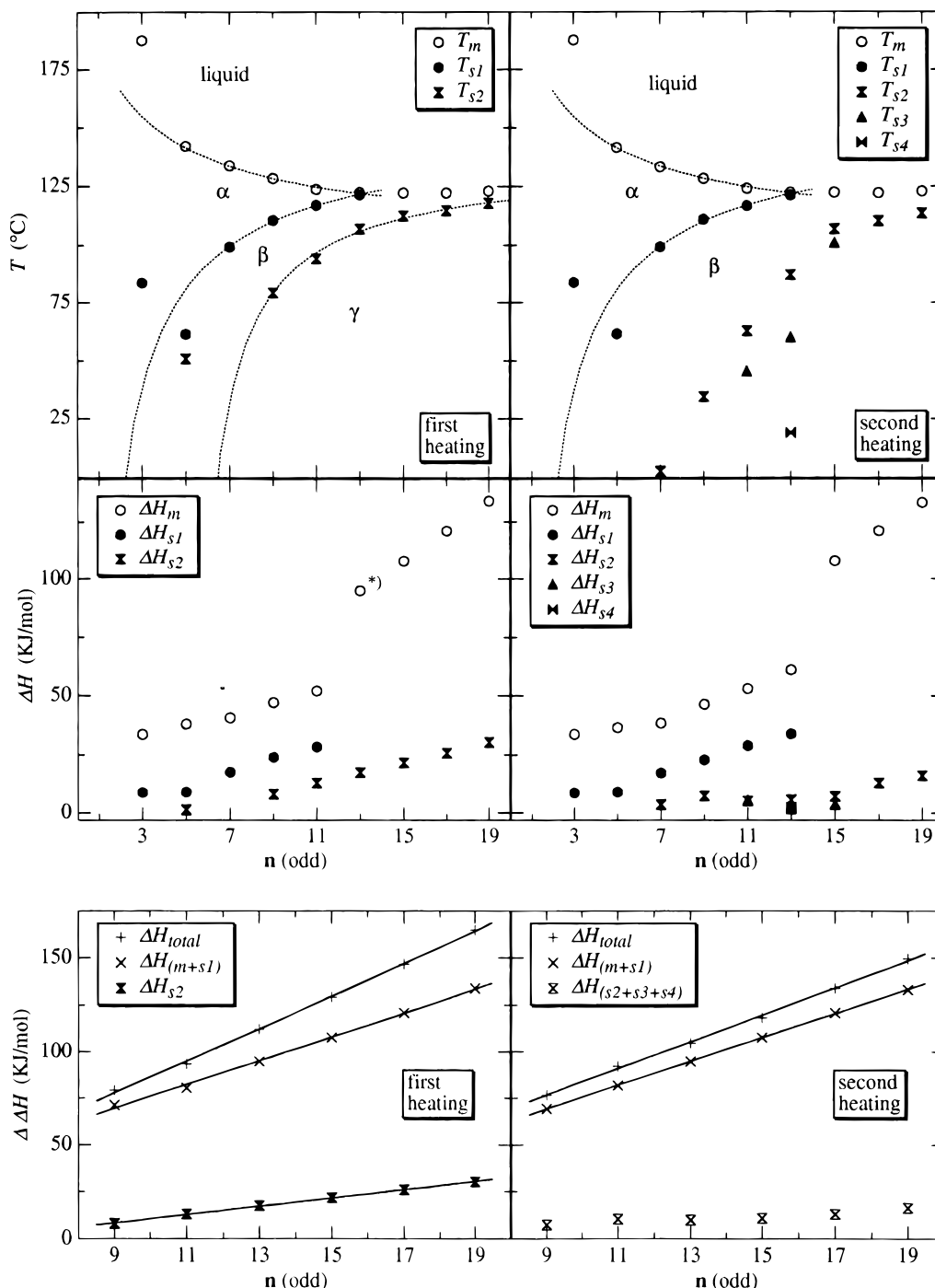Chem. Mater., Vol. 8, No. 5, 1996   1097

Figure 3. Thermal behavior of compounds **1(*n*)** with odd number of carbon atoms per alkyl chain: (a, top) Phase transition temperatures with the related enthalpy changes present in first and second heating run together with the calculated hyperbolic relationships. (b, bottom) Linear relationships in the enthalpy changes dependence on the alkyl chain length for $n \geq 9$.

Table 4. Intercepts ΔH° (kJ mol^{-1}) and ΔS° (J K^{-1} mol^{-1}) and Increments ΔH (kJ mol^{-1}) and ΔS (J K^{-1} mol^{-1}) Values of the Linear Relationships in the Odd ($9 \leq n \leq 19$) and Even ($10 \leq n \leq 18$) Series, Respectively

| series | transitions | first heating run | | | | | | second heating run | | | | | | |
		ΔH°	ΔH	R^2	ΔS°	ΔS	R^2	transitions	ΔH°	ΔH	R^2	ΔS°	ΔS	R^2
odd	total	−0.10	8.65	0.999	5.63	21.55	0.999	total	12.6	7.18	0.999	41.9	17.56	0.998
	m + s1	11.99	6.40	0.998	30.65	16.14	0.998	m + s1	11.5	6.42	1	29.6	16.19	1
	s2	−11.53	2.21	0.999	−25.01	5.40	0.999	m^a	12.29	3.74	0.998	25.18	9.92	0.999
								$s1^a$	−1.93	2.77	0.999	0.79	6.58	0.998
even	total	−25.04	9.16	0.994	−66.51	23.72	0.993	total	−9.63	7.30	0.95	−13.87	18.01	0.93
	m + s1	1.62	6.31	0.999	3.26	16.12	0.999	m + s1	−12.30	5.81	0.992	−3.03	16.06	0.993

^{a} Least-squares fits through enthalpy and entropy changes at $n = 7$, 9, 11, and 13 (second heating run).

transition **s2**, $\gamma \rightarrow \beta$ of pristine **1(*n*)**, the linear increments ΔH_{s2} and ΔS_{s2} are ca. 25% of H_{total} and S_{total}, respectively. The latter indicates that the alkoxy chains

gain considerable mobility (Table 4). On the basis of the linear relations calculated for ΔH_m, ΔS_m, ΔH_{s1}, and ΔS_{s1} taken from the second heating runs and their

Table 5. Comparison of Intercepts ΔH° (kJ mol^{-1}) and ΔS° (J K^{-1} mol^{-1}), and Increments ΔH (kJ mol^{-1}) and ΔS (J K^{-1} mol^{-1}) Values^a of 1(n) with n-Alkanes^b at Distinct Phase Transitions

compound	n	phase transition	ΔH°	ΔS°	ΔH	ΔS
1(n)	odd: $9 \leq n \leq 19$	triclinic^c to isotropic liquid	-0.1	8.7	4.33	10.8
n-alkane	even: $6 \leq n \leq 24$	triclinic to isotropic liquid	-11.7	10.7	4.07	10.7
n-alkane	odd: $11 \leq n \leq 37$	orthorhombic to isotropic liquid	-12.1	16.5	3.74	9.4
n-alkane	odd: $11 \leq n \leq 37$	hexagonal to isotropic liquid	3.8	28.3	2.49	6.0

^{a} Values for one alkyl chain. ^{b} See refs 44 and 45. ^{c} Pristine material (γ-phase).

reversibility (n = 7, 9, 11, and 13), ΔH_{s1} and ΔS_{s1} are estimated to be ca. 32% of ΔH_{total} and ΔS_{total}, respectively, from the first heating run. Thus, in the α-phase the alkoxy chains possess ca. 57% of their total configurational entropy, which is higher than the configurational entropy of n-alkanes in their rotator phase (ca. 45%).[45−49] This provides evidence for the presence of attractive forces between the 1,4-benzoquinone units which prevents them from melting and is supported by their T_m dependence concomitant with the value of n (vide infra). At melting the total amount of entropy gained per CH$_2$ group (10.8 J K^{-1} mol^{-1}) approximates the calculated statistical entropy (9.1 J K^{-1} mol^{-1}). Hence, a random configuration of alkoxy chains is expected in the molten state.[24,47]

Insight in the changes of both 1,4-benzoquinone packing and alkyl endgroup packing in the distinct phases is derived from the intercepts ΔH° and ΔS°. At the transition **s2**, $\gamma \rightarrow \beta$ of pristine **1(n)** a denser 1,4-benzoquinone and/or the end-group packing is anticipated based on the negative values of ΔH°_{s2} (-11.53 kJ mol^{-1}) and ΔS°_{s2} (-25.01 J K^{-1} mol^{-1}). At melting the positive ΔH°_m (12.29 kJ mol^{-1}) and ΔS°_m (25.18 J K^{-1} mol^{-1}) values reflect the breaking of attractive forces between the 1,4-benzoquinone moieties (see Table 4, second heating run).

In the case of a linear relation between alkoxy chain length with enthalpy and entropy changes at a phase transition, the phase transition temperature as a function of alkoxy chain length has to obey a hyperbolic function (eq 4):[24,47]

$$T = \frac{\Delta\Delta H}{\Delta\Delta S} = \frac{\Delta H^\circ + n\Delta H}{\Delta S^\circ + n\Delta S} = \frac{\Delta H}{\Delta S}\left(1 + \frac{\Delta H^\circ/\Delta H - \Delta S^\circ/\Delta S}{n + \Delta S^\circ/\Delta S}\right) \quad (4)$$

with asymptotic lines $T = \Delta H/\Delta S$ and $n = -\Delta S^\circ/\Delta S$. Note that in the case of $\Delta H^\circ/\Delta H > \Delta S^\circ/\Delta S$ a decreasing hyperbolic curve is found, while for $\Delta H^\circ/\Delta H < \Delta S^\circ/\Delta S$ it increases. In Figure 3, the calculated hyperbolic curves for the second and the first solid−solid phase transition are drawn for pristine compounds **1(n)**. This gives additional proof for the presence of identical structures within these series before and after the transition. The strong increase of T_{s1} and T_{s2} with n (9 $\leq n \leq$ 19), which is reminiscent of the thermal behavior of n-alkanes,[43] demonstrates the dominant influence of the n-alkyl chains ($\Delta H^\circ/\Delta H < \Delta S^\circ/\Delta S$). The decrease of T_m for $3 \leq n \leq 13$ shows that T_m is dominated by the melting of the rigid 1,4-benzoquinone moiety ($\Delta H^\circ/\Delta H > \Delta S^\circ/\Delta S$).

*Analysis of the Thermal Properties of **1(n)** with n = Even.* Although less ideal, the thermal behavior in the even series resembles that of odd compounds **1(n)**. In the first and second DSC heating curves **1(n)** with $4 \leq n \leq 18$ showed one pronounced solid−solid phase transition. For **1(n)** with $n = 4$ and $12 \leq n \leq 18$ additional minor solid−solid phase transitions are observed. Subsequent cooling and heating runs revealed that for $n > 10$ irreversible behavior of the solid−solid phase transitions. Compounds **1(n)** with short alkoxy chains ($n \leq 10$) possess reversible thermal behavior. Analogous to **1(3)**, **1(2)** and **1(4)** differ from the higher homologues. Linear relationships between n and $\Delta\Delta H$ and $\Delta\Delta S$ are found for $10 \leq n \leq 18$ (cf. eqs 2 and 3): (i) the total sum of enthalpy and entropy changes at the different transitions (ΔH_{total} and ΔS_{total}, Table 4) and (ii) the sum of the enthalpy and entropy changes at melting and the first solid−solid phase transition ($\Delta H_{(m+s1)}$ and $\Delta S_{(m+s1)}$).

This suggests identical solid-state packing for pristine **1(n)** at ambient temperature as well as in the β-phase. Although the linear increments ΔH_{total} (9.16 kJ mol^{-1}) and ΔS_{total} (23.72 J K^{-1} mol^{-1}) are slightly higher than those found in the odd series, a resemblance in alkoxy chain packing between the even and odd series at room temperature is expected (Table 4). This is corroborated by the increment values of $\Delta H_{(m+s1)}$ (6.42 kJ mol^{-1}) and $\Delta S_{(m+s1)}$ (16.19 J K^{-1} mol^{-1}) which are close to those found in the odd series [increment values, $\Delta H_{(m+s1)}$ (6.40 kJ mol^{-1}), $\Delta S_{(m+s1)}$ (16.14 J K^{-1} mol^{-1})].[50] Hence, the differences between the intercept values ΔH°_{total}, ΔS°_{total}, $\Delta H^\circ_{(m+s1)}$, and ΔH°_{total} of the odd and even series are remarkable (see Table 4). They suggest considerable differences in density of the alkoxy chain end-group packing. This is corroborated by density measurements (vide infra). The large negative differences between ΔH°_{total} even (-25.04 kJ mol^{-1}) and ΔH°_{total} odd (-0.10 kJ mol^{-1}) of -24.94 kJ mol^{-1} and ΔS°_{total} even (-66.51 J K^{-1} mol^{-1}) and ΔS°_{total} odd (5.63 J K^{-1} mol^{-1}) of -72.14 J K^{-1} mol^{-1} implies an additional free volume contribution due to end-group packing of pristine **1(n)** with n is even. In the β-phase these differences between the even and odd series ($\Delta\Delta H^\circ_{(m+s1)} = -10.37$ kJ mol^{-1}, $\Delta\Delta S^\circ_{(m+s1)} = -27.39$ J K^{-1} mol^{-1}) are reduced, which indicates that the end-group packing improves at the minor phase transitions (**s2**, $\gamma \rightarrow \beta$ and/or **s3**, $\delta \rightarrow \gamma$) for n is even.

From the second DSC heating runs a linear relation is obtained between n and both the sum of enthalpy and entropy changes at melting and the first solid−solid phase transition (**s1**, $\beta \rightarrow \alpha$). The increment values of $\Delta H_{(m+s1)}$ (5.81 kJ mol^{-1}) and $\Delta S_{(m+s1)}$ (16.06 J K^{-1} mol^{-1}) are slightly smaller which point to difficulties in the

(46) In this phase the alkoxy chains are packed in hexagonal crystal structures and possess rotational freedom along the long crystal axis.

(47) Ubbelohde, A. R. *The Molten State of Matter, Melting and Crystal Structure*; John Wiley & Sons: Chichester, 1978, and references therein.

(48) Maroncelli, M.; Qi, S. P.; Straus, H. L.; Snyder, R. G. *J. Am. Chem. Soc.* **1982**, *104*, 6237.

(49) McClure, D. W. *J. Chem. Phys.* **1968**, *49*, 1830.

(50) No linear relation is found for the enthalpy changes and entropy changes at the transition from the β- to α-phase. Therefore in contrast with the odd series, structural differences exist in the α-phase with $10 \leq n \leq 18$. This is confirmed by the increase of melting enthalpy with n (see Figure 4).

Self-Organization in the Solid State
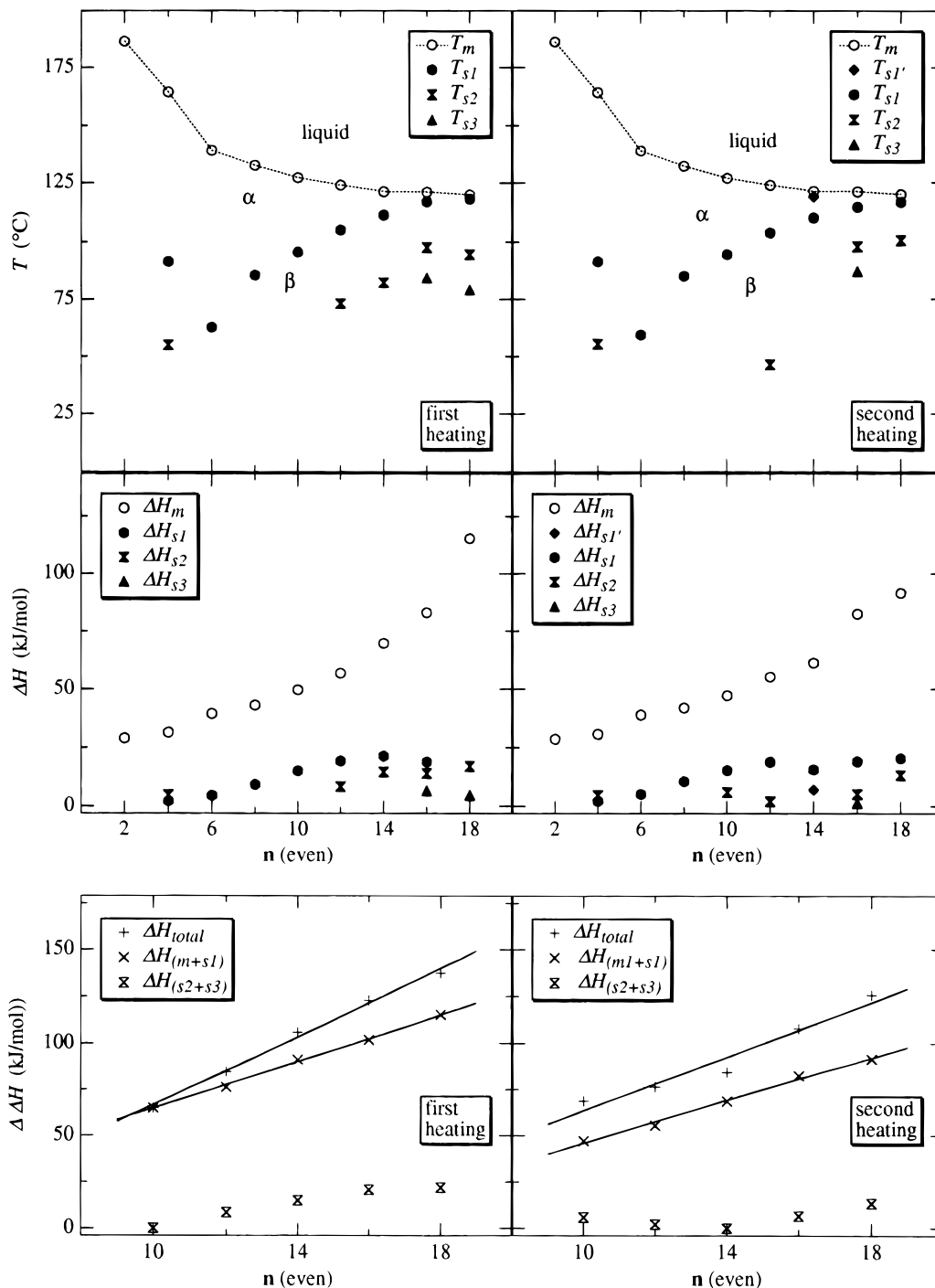
Chem. Mater., Vol. 8, No. 5, 1996 1099

Figure 4. Thermal behavior of compounds **1(n)** with even number of carbon atoms per alkoxy chain: (a, top) Phase transition temperatures with the related enthalpy changes present in first and second heating run. (b, bottom) Linear relationships for $n \geq 10$ in the enthalpy changes dependence of the alkoxy chain length.

reversibility of alkoxy chain packing. Since the intercepts $\Delta H^{\circ}_{(m+s1)}$ (-12.30 kJ mol^{-1}) and $\Delta S^{\circ}_{(m+s1)}$ (-3.03 J K^{-1} mol^{-1}) differ from those obtained from the first DSC heating curves, it can be concluded that this is due to hindered end-group packing (see Table 4).

Density Measurements. Density measurements (picnometry)[26] provide additional insight in the odd−even effects found with DSC (Figure 5a, Table 2). For **1(9)** and **1(10)** the picnometric data are in excellent agreement with the calculated values (single-crystal X-ray data, Table 1; deviations ≤ 0.01 g/cm^3 (vide infra)). In the case of **1(3)** picnometry gives a density which is 0.03 g cm^3 smaller than the calculated value; this is

attributed to the fact that the single-crystal X-ray structure was determined at 150 K.

Since in the homologous series **1(n)** molecular weight increases linearly with alkoxy chain length and the DSC data indicate that the higher homologues possess identical packing, linear relationships are also expected between alkoxy chain length and molecular volume (V, eq 5):

$$\frac{M_w}{dN_A} = V^{\circ} + nV \qquad (5)$$

with d being the density, N_A Avogadro's number, V° the intercept representing the volume of a 2,5-dioxy-1,4-
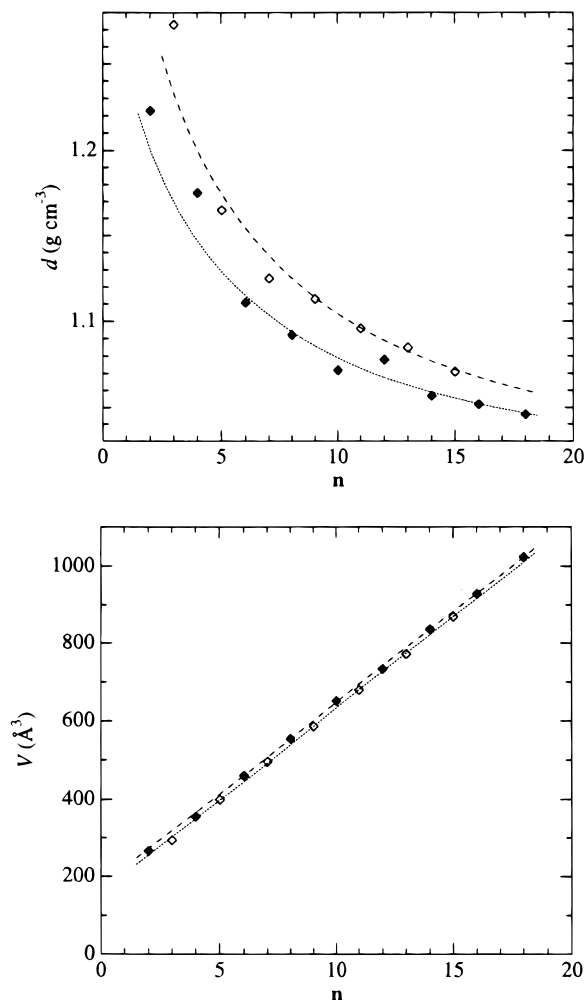
Figure 5. (a, top) Density of compounds **1(*n*)** measured by picnometry; the calculated hyperbolic dependence of the density from the carbon number *n* in the odd ($9 \leq n \leq 15$) and even series ($10 \leq n \leq 18$) is displayed. (b, bottom) Linear dependency of molecular volume of **1(*n*)** upon *n*.

benzoquinone-type moiety and additional contributions from alkoxy chain end-group packing, and *V* the linear volume increment per two CH_2 groups. Moreover, if eq 4 applies, *d* has to fulfill a hyperbolic function (eq 6):

$$d = \frac{M^\circ + nM}{N_A(V^\circ + V)} = \frac{M}{N_A V}\left(1 + \frac{M^\circ/M - V^\circ/V}{n + V^\circ/V}\right) \quad (6)$$

M° represent the molecular weight of 2,5-dioxy-1,4-benzoquinone moiety and two hydrogen atoms and *M* the molecular weight increment per two CH_2 groups.

In agreement with the DSC results for both the odd ($9 \leq n \leq 15$) and even ($10 \leq n \leq 18$) series linear as well as hyperbolic dependencies are found (Figure 5). The *V* and V° values in both the odd and even series are in line with those calculated from the single-crystal X-ray data of **1(9)** and **1(10)** (Table 6). Note that the odd-even alternation in *V* is due to an increase of V° for the even series; i.e., *V* being nearly equal for both series. ΔV° equals 17.1 Å^3, which is in excellent agreement with the difference (18.3 Å^3) between **1(9)** and **1(10)** derived from the single-crystal X-ray data. This supports our contention that the difference between the odd and even ΔS°_{total} values is related to additional free volume in even series. In line with their different thermal behavior, the densities of compounds with short alkoxy chains

Table 6. Comparison of V (Å^3) and V° (Å^3) Values of 1(*n*) Derived from Single-Crystal X-ray Analysis (1(9) and 1(10)) and the Linear Relationship between the Molecular Volume V and Alkoxy Chain Length[a]

series	**1(*n*)**	V°	V	R^2
odd	**1(9)**[b]	158.6	47.21	
	$9 \leq n \leq 15$[c]	160.1	47.24	1
even	**1(10)**[b]	176.9	46.83	
	$10 \leq n \leq 18$[c]	177.2	47.02	0.999

[a] V is the average volume of two CH_2 groups and V° represents the volume of 2,5-dioxy-1,4-benzoquinone moiety and additional end-group contributions of the alkoxy chains. [b] Single-crystal X-ray data. [c] Picnometry (see text).
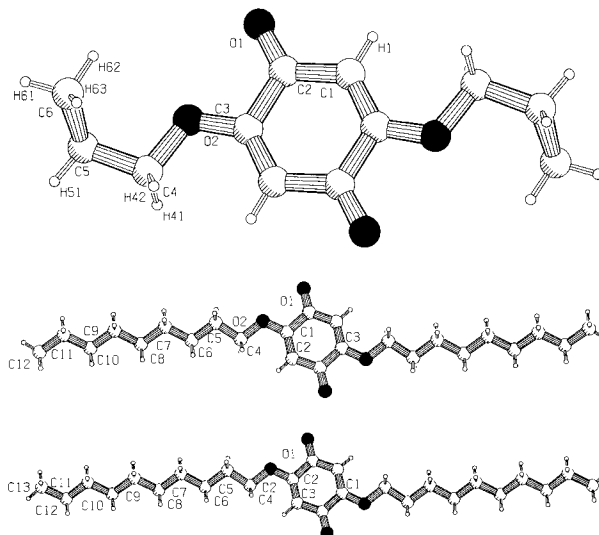

Figure 6. PLUTON representations of (top) 2,5-di-*n*-propoxy-1,4-benzoquinone **(1(3))**, (middle) 2,5-di-*n*-nonoxy-1,4-benzo-quinone **(1(9))**, and (bottom) 2,5-di-*n*-decyloxy-1,4-benzoquino-ne **(1(10))**.

deviate. This suggests that they possess different packing motifs. The relative high densities of compounds **1(2)**, **1(3)**, and **1(4)** are indicative of efficient molecular packing. The relatively lower density of **1(7)** demonstrates the lower density of the β-phase compared to γ-phase of the higher odd analogues (cf. DSC results). Considering the more complex thermal behavior in the even series the calculated hyperbolic curve for these series describes remarkably well the density dependence upon alkoxy chain length. The average density of alkoxy chain packing given by the horizontal asymptotic line is 1.014 and 1.009 g/cm^3 for the odd and even series, respectively. These values are slightly higher than the density of polyethylene (0.96 g/cm^3).[24]

Single-Crystal X-ray Structures of 2,5-Di-*n*-pro-poxy-1,4-benzoquinone (1(3)), 2,5-Di-*n*-nonyloxy-1,4-benzoquinone (1(9)), and 2,5-Di-*n*-didecyloxy-1,4-benzoquinone (1(10)). Compounds **1(3)**, **1(9)**, and **1(10)** crystallize in the space group $P\bar{1}$ with one molecule per unit cell (Table 1). PLUTON representations, salient bond lengths, and valence angles are given in Figures 6 and 7, respectively. For both **1(3)**, **1(9)**, and **1(10)** nearly identical 1,4-benzoquinone structures are observed. They are nearly planar (maximum deviation from least-squares plane amounts to 0.0009(4), 0.013(2), and 0.017(3) Å for **1(3)**, **1(9)**, and **1(10)**, respectively). Due to the presence of the alkoxy substituents the 1,4-benzoquinone skeleton possesses a
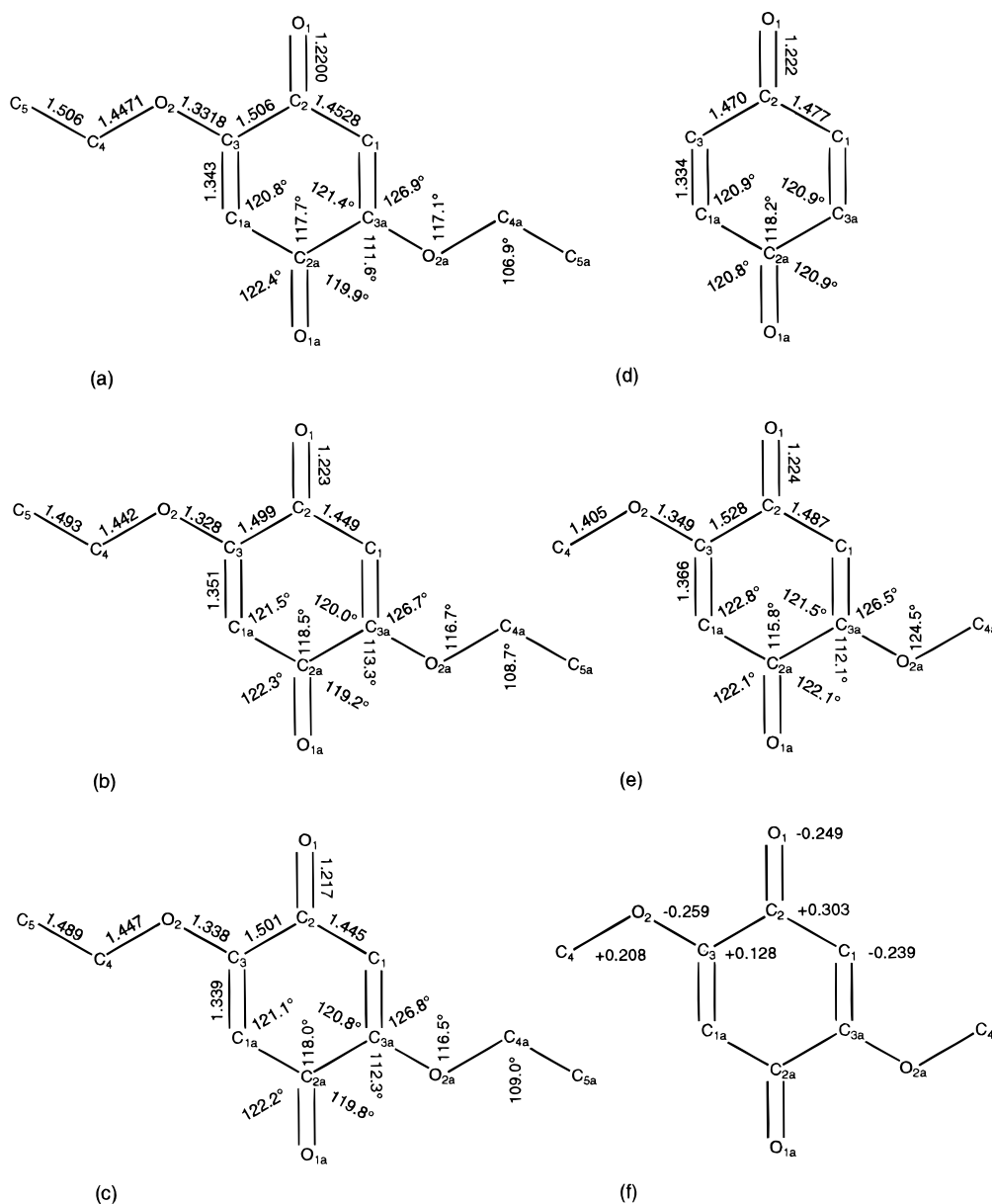
Figure 7. Experimental (single-crystal X-ray data) [(a) **1(3)**, (b) **1(9)**, (c) **1(10)**, and (d) 1,4-benzoquinone[52]] and calculated (MOPAC 6.0; MNDO) bond lengths (Å) and angles (deg) [(e) **1(1)**]; (f) MNDO total atomic charges in q calculated for **1(1)**.

merocyanine-like distortions,[51] i.e., bond equalization along two 6π-electron/5-center perimeters [O(1)−C(2)−C(1)−C(3a)−O(2a) and O(1a)−C(2a)−C(1a)−C(3)−O(2)] is discernible (cf. refs 21 and 22). The single C−C bonds at both sides of the carbonyl group differ ca. 0.05 Å (**1-(3)**; 0.053(3) Å, **1(9)**; 0.050(5) Å and **1(10)**; 0.056(6) Å). Compared to 1,4-benzoquinone[52] a contraction of C(1)−C(2) of 0.025 Å and an elongation of the C(2)−C(3) of 0.025 pm is observed (Figure 7). Although the sum of valence angles (Σ) around C(3) is 360°, they deviate from 120° (C(2)−C(3)−O(2) = 112.3° and C(1a)−C(3)−O(2) = 126.8°) indicative for the occurrence of substantial rehybridization.[51]

Directional weak contacts between quinoid hydrogens and carbonyl oxygens of adjacent 1,4-benzoquinones leads to the formation of infinite ribbon-type structures
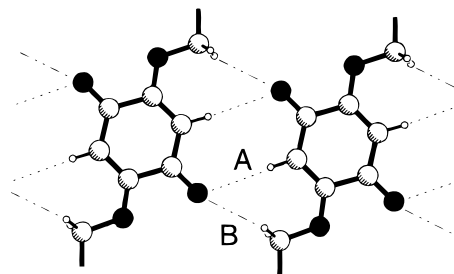

Figure 8. Schematic representation of the ribbon-type structures present in the packings motifs of **1(3)**, **1(9)**, and **1(10)** as results of weak C−H···O interactions; distances *A* and *B* are reported in Table 7.

for **1(3)**, **1(9)**, and **1(10)** (Figure 8 and Table 7). The quinoid H···O(=C) distance equals the sum of the van der Waals radii minus 0.22, 0.10, and 0.16, respectively (isotropic radii;[53] C 1.70, H 1.20, O 1.52 Å). In line with common criteria for linear C−H···O bonds,[54−56] the

(51) Bock, H.; Ruppert, K.; Näther, C.; Havlas, Z.; Herrmann, H.-F.; Arad, C.; Göbel, I.; John, A.; Meuret, J.; Nick, S.; Rauschenbach, A.; Seitz, W.; Vaupel, T.; Solouki, B. *Angew. Chem., Int. Ed. Engl.* **1992**, *31*, 550 and references therein.
(52) Bolhuis, F.; Kiers, C. Th. *Acta Crystallogr.* **1978**, *B34*, 1015.

(53) Bondi, A. *J. Phys. Chem.* **1964**, *68*, 441.

Table 7. Salient Intermolecular Hydrogen Contacts for 1(3), 1(9), and 1(10)

compound	H···O contact	direction	$d_{H···O}$ (Å)	$\Delta_{sum}{}^a$ (Å)	$d_{C···O}$ (Å)	$\angle_{H···C=O}$ (deg)	$\angle_{C-H···O}$ (deg)
1(3)	quinoid H···O=C; [A]^c	[1 −1 0]^b	2.501	−0.22	3.453	116.8	173.6
	H(42)···O(2); [C]^c	[1 0 0]	2.590	−0.13	3.558		157.8
1(9)	quinoid H···O=C; [A]^c	[1 −1 0]^b	2.617	−0.10	3.540	115.3	172.0
	H(41)···O=C; [B]^c	[1 −1 0]^b	2.600	−0.12	3.213	159.6	121.3
	H(42)···O=C; [D]^c	[0 1 0]	2.687	−0.03	3.213	108.7	153.1
1(10)	quinoid H···O=C; [A]^c	[1 1 0]^b	2.556	−0.16	3.531	115.5	173.3
	H(41)···O=C; [B]^c	[1 1 0]^b	2.594	−0.13	3.214	159.7	121.3
	H(42)···O=C; [D]^c	[0 1 0]	2.680	−0.04	3.214	108.8	152.9

^{a} Δ_{sum} = distance $d_{H···O}$ minus sum of the van der Waals radii = 2.72 Å [isotropic radii; H = 1.20 Å and O = 1.52 Å]. ^{b} Lateral hydrogen contacts positioned in the ribbon plane. ^{c} See Figure 8 and/or Figure 11.

hydrogen atoms are directed toward a lone pair of the carbonyl oxygen (C=O···H 116° and C−H···O 173°). In the case of **1(9)** and **1(10)** additional close hydrogen contacts are found in the ribbon planes between methyl hydrogen H(41) and the carbonyl oxygens (Figure 8 and Table 7). Although the H···O distances are either smaller or equal to the sum of the van der Waals radii minus 0.12 Å, the directionality of these bonds deviates from criteria for linear hydrogen bonds (C=O···H 160° and C−H···O 121°).

Compounds **1(3)**, **1(9)**, and **1(10)** possess a solid-state packing motif of one-dimensional ribbons in which the different parts, i.e., the alkoxy chains and the rigid 1,4-benzoquinone skeleton, occupy separated domains (Figure 9). Within a ribbon the 1,4-benzoquinone units display a staircaselike motif with perpendicular distances between least-square planes through adjacent 1,4-benzoquinone units of 0.14, 0.26, and 0.25 Å for **1-(3)**, **1(9)**, and **1(10)**, respectively. Note that there is no close packing of the alkoxy chains in the ribbon plane due to crystallographic incommensurability of the 2,5-dioxy-1,4-benzoquinone subunit and the aliphatic chains. The subsequent one-dimensional layer is packed slightly shifted on top leading to a close packing of the alkoxy chains and minimalization of intermolecular dipole−dipole interactions (in the *a* direction O(1)−C(2)−C(1)−C(3a) is positioned *antiparallel* above C(3)−C(1a)−C(2a)−O(1a) of an adjacent molecule (perpendicular distance of **1(3)** 3.35 Å, **1(9)** and **1(10)** 3.48 Å, Figure 10).[21,22]

Although the alkoxy chains of **1(9)** and **1(10)** are close to antiperiplanar, a torque is present in the vicinity of the 1,4-benzoquinone unit; torsion angles which deviate from the ideal value of 180° are found (Table 8, see footnote). Similar values are found for **1(9)** and **1(10)** (torsion angle C(3)−O(2)−C(11)−C(12) **1(9)** 34.5° and **1(10)** 31.9°). A cross section through C(8) and C(7) shows a triclinic-type packing motif (Figure 9d). Note that the average subcell for the alkoxy chains deviates only moderately from that for an ideal triclinic packing motif (Table 9).[57] The *a* axis is shortened by 0.1 Å and the *b* axis is lengthened by 0.2 Å. This is in line with the DSC data. In the case of **1(3)** the alkoxy chains are too short and the incommensurability is apparently resolved by the introduction of gauche kinks present at the end of the propyl chains (Figure 9a). The one-dimensional planes combine into a two-dimensional
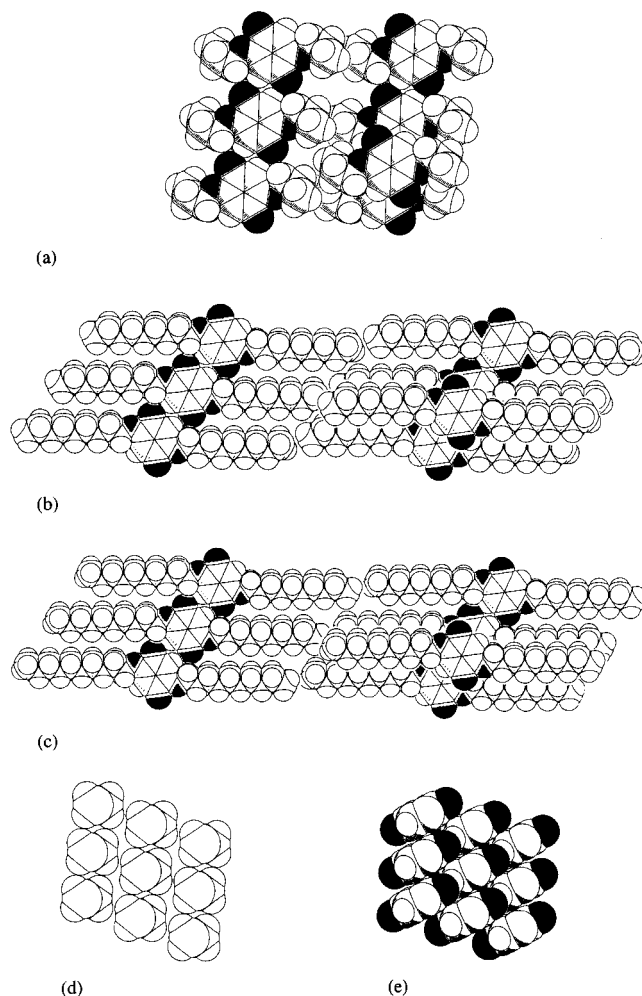
(54) Desiraju, G. R. *Acc. Chem. Res.* **1991**, *24*, 290.
(55) Berkovitch-Yellin, Z.; Leiserowitz, L. *Acta Crystallogr.* **1984**, *840*, 159.
(56) Jeffrey, G. A.; Maluszynska, H.; Mitra, J. *Int. J. Biol. Macromol.* **1985**, *7*, 336.
(57) Kitaigorodsky, A. I. *Molecular Crystals and Molecules*; Academic Press: New York, 1973; p 48 and references therein.

Figure 9. CPK representations showing the solid-state packing motif of **1(3)**, **1(9)**, and **1(10)**. Lamellar alkoxy chain packing: (a) **1(3)**, (b) **1(9)**, and (c) **1(10)**. (d) Cross section through the alkoxy chain packing of **1(9)** and **1(10)** showing C(8) and C(7). (e) Schematic representation of the 1,4-benzoquinone packing of **1(9)** and **1(10)** viewed in the same direction as Figure 9d; *n*-alkoxy chains are omitted for clarity.

layered structure with columnar stacked benzoquinone moieties along the *a* and *b* axes (Figures 9e and 11).

Center-to-center and perpendicular distances are reported in Table 10. These parameters show that alkoxy chain length hardly influences the efficacy of this architecture. The center-to-center distance in the *a* direction (4.2 Å) which is close to the *a* axis together with a tilt angle of ca. 34° indicates favorable π-overlap (shown for **1(9)** in Figure 10; identical molecular overlap was observed for **1(3)** and **1(10)**). In the *b* direction the center-to-center distance is ca. 5.3 Å with a tilt angle of ca. 53°. For **1(3)** linear weak hydrogen interactions are present between the hydrogen atoms H(42) and oxygen
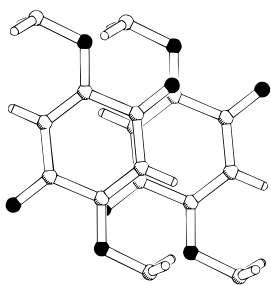
Figure 10. Plane-to-plane molecular overlap of **1(9)** in the *a*-axis direction showing the directional force of the inter-molecular dipole−dipole interactions; viewed perpendicular to the 1,4-benzoquinone plane. For **1(3)** and **1(10)** an identical molecular overlap was found.
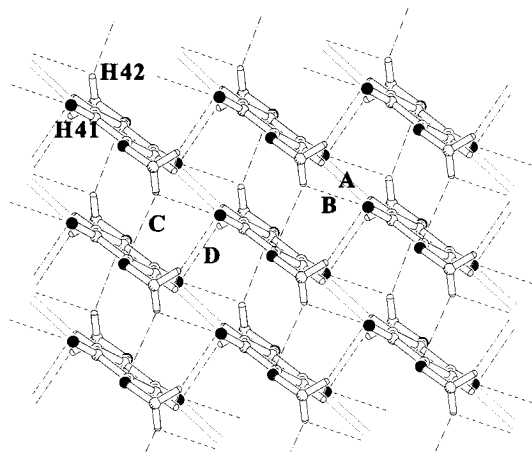

Figure 11. Schematic representation of the two-dimensional columnar structure of **1(3)**, **1(9)**, and (c) **1(10)**; alkoxy chains are omitted for clarity. Weak hydrogen contacts [*A*, *B*, *C*, and *D*] are represented by broken lines (Table 7).

Table 8. Selected Torsion Angles (deg) of the Alkoxy Chain Conformation of 1(3), 1(9), and 1(10)[a]

torsion angle	1(3)	1(9)	1(10)
C(2)C(3)O(2)C(4)	−176.5	177.5	177.0
C(3)O(2)C(4)C(5)	173.8	174.7	177.0
O(2)C(4)C(5)C(6)	−58.4	169.0	169.2
C(4)C(5)C(6)C(7)		171.6	172.4
C(5)C(6)C(7)C(8)		176.7	176.7
C(6)C(7)C(8)C(9)		177.1	177.0
C(7)C(8)C(9)C(10)		178.5	177.2
C(8)C(9)C(10)C(11)		178.8	179.2
C(9)C(10)C(11)C(12)		179.1	179.4
C(10)C(11)C(12)C(13)			−179.5

[a] The atom numbering of **1(9)** is also used for **1(3)** and **1(10)** (see Figure 6).

Table 9. Average Subcell Calculated for Triclinic Alkoxy Chain Packing of 1(9) and 1(10)

parameter	reference	1(9)	1(10)
a (Å)	4.3	4.20	4.21
b (Å)	4.45	4.76	4.72
c (Å)	2.54	2.55	2.54
α (deg)	90.0	88.91	89.34
β (deg)	107.5	107.74	107.68
γ (deg)	102.0	102.84	102.86
V_{calc} (Å³)	45.2	47.21	46.83

atoms of the *n*-alkoxy substituents in the *a* direction (Figure 11 and Table 7). The higher analogues **1(9)** and **1(10)** possess close hydrogen contacts between hydrogen atoms H41 and the carbonyl oxygens in the *b* direction. For the latter this contact only equals the sum of the van der Waals radii minus 0.04 Å. Nevertheless, they

Table 10. Column Parameters of 1(3), 1(9), and 1(10)

parameter	1(3)	1(9)	1(10)
Center-to-Center Distance (Å)			
a direction	4.2258	4.1996	4.2118
b direction	5.1429	5.3552	5.3337
Interplanar Distance[a] (Å)			
a direction	3.345	3.482	3.479
b direction	3.209	3.223	3.233
Tilt Angle[b] (deg)			
a direction	37.67	33.99	34.31
b direction	51.39	53.00	52.69

[a] Perpendicular distance between successive 1,4-benzoquinone moieties. [b] Angle between the normal on the 1,4-benzoquinone plane and the stacking axis (=center-to-center vector).

are in line with the directional criteria for linear hydrogen bonds (Figure 11 and Table 7).

As shown above, **1(9)** and **1(10)** possess almost identical molecular structures and their alkyl packing induces identical two-dimensional packing motifs. The subsequent assembly of these layers giving the three-dimensional crystal displays a difference. Although the calculated subcell volumes through methyl end groups of **1(9)** (59.15 Å³) and **1(10)** (58.91 Å³) are equal, the volumes of a subcell through the CH_2CH_3 end groups are substantially different viz. 88.17 and 124.56 Å³, respectively; a denser end-group packing is observed for **1(9)** which contains an odd number of carbon atoms per alkyl chain (see Figure 9b,c).

Powder WAXD Analysis. To complement the DSC and single-crystal X-ray analyses, powder wide-angle X-ray diffraction (WAXD) patterns of compounds **1(*n*)** were recorded at ambient temperature. In line with the reversible thermal behavior observed with DSC, compounds **1(*n*)** with short alkoxy chains ($n \leq 8$ and $n = 10$) show identical WAXD patterns before and after annealing. However, for higher analogues ($n = 9$ and $n \geq 11$) they are different. In the powder X-ray diagrams the (001) and higher order reflections can be readily identified since they are located in the small reflection angle region (4θ; ($0° < 4\theta < 30°$)) due to the fact that compounds **1(*n*)** possess an oblong shape. The long spacing distance ($1/|\boldsymbol{c^*}|$; Tables 2 and 3) represents the perpendicular distance between adjacent two-dimensional molecular layers. Analysis of the interlayer distance concomitant with the alkyl chain length shows that in both the odd and even series linear relations are found between $1/|\boldsymbol{c^*}|$ and *n* both before and after annealing (Figure 12). Note the odd−even alternation in the interlayer distance dependence of *n*; the odd $1/\boldsymbol{c^*}$ values are relatively higher. Furthermore, different linear relationships for the lower ($n < 9$) and higher ($n \geq 9$) homologues are observed for both series. This is in line with the DSC data which revealed a different thermal behavior for the lower and higher analogues. It should be pointed out that the slope of the lines through the odd and even pristine representatives are nearly identical, i.e., 2.10 and 2.09 Å. This suggests similar alkoxy chain packings in both series. Again different intercepts are found indicative for less efficient end-group packing in the even series (vide supra). After annealing, the slope increases to 2.18 and 2.17 Å, respectively, demonstrating slightly different packing of the higher analogues after crystallization from the molten state.

For pristine **1(*n*)** the WAXD patterns possess large similarities within the odd ($9 \leq n \leq 19$) and even ($12 \leq$

Figure 12. Interlayer distance as a function of the alkoxy chain length for pristine and annealed **1(*n*)**.

Figure 13. Schematic representation of diffraction patterns of the even pristine series (10 ≤ *n* ≤ 18) between 0° < 4θ < 70° and the calculated pattern of **1(10)**; lines with an intensity >2% are displayed; different intensities are depicted by bold (strong), normal (medium), and thin lines (weak).

Figure 14. Schematic representation of the powder WAXD patterns of the odd pristine series (9 ≤ *n* ≤ 19) between 0° < 4θ < 70°; lines with an intensity >2% are displayed; different intensities are depicted by bold (strong), normal (medium) and thin lines (weak).

n ≤ 18) pristine series. Even after thermal treatment the WAXD patterns were almost identical in odd (9 ≤ *n* ≤ 19) and in the even (12 ≤ *n* ≤ 18) series. To identify the reflections within the pristine odd (9 ≤ *n* ≤ 19) and even (12 ≤ *n* ≤ 18) series, we have calculated the WAXD patterns using the single-crystal X-ray data of **1(9)** and **1(10)**. The calculated diffractogram of **1(9)** is in excellent agreement with its experimental powder diffraction pattern. Surprisingly, the calculated diffraction pattern of **1(10)** differs from the WAXD pattern of pristine **1-(10)**. The latter resembles the experimental WAXD pattern of pristine **1(12)** and higher analogues (Figure 13). This is attributed to polymorphism and more specific related to differences in endgroup packing. Crystals for single-crystal X-ray analysis were obtained by crystallization from a slowly evaporating CH_2Cl_2/ THF solution (ambient temperature, 2 weeks) while bulk pristine **1(10)** was obtained from a saturated THF solution (−20 °C, 4 h). As illustrated for the odd pristine **1(*n*)** with 9 ≤ *n* ≤ 19, the observed reflections shift systematically with increasing alkyl chain length (Figure 14). Hence, we conclude that within this series compounds **1(*n*)** have to possess crystal structures identical with that of **1(9)**. Their unit-cell dimensions differ in length of the *c* axis and small changes of α and β. The *a* (4.20 Å) and *b* axis (5.355 Å) and angle between them (γ = 86.98°) are constant within the series. The same applies for the pristine even series

(12 ≤ *n* ≤ 18); they possess crystal structures identical with the single-crystal X-ray structure of **1(10)** (*a* = 4.212, *b* = 5.334, γ = 92.99°). Also after thermal treatment identical crystal structures are present within both the odd (9 ≤ *n* ≤ 19) and even (12 ≤ *n* ≤ 18) series. Noteworthy, the calculated powder diffraction patterns from **1(9)** and **1(10)** differ despite the fact that they have nearly identical two-dimensional structures (see the single-crystal X-ray analysis and Figure 13). Although comparable *hkl* reflections are present in both diffractograms, their intensities and positions are different due to different end-group packing.

For a triclinic cell the following direct/reciprocal relationship has to apply (eq 7):[58]

$$|c^*| = \frac{|a||b| \sin \gamma}{V} \tag{7}$$

with V being the cell volume. Under the assumption that for the homologues a, b, and γ are constant within both the odd and even series, the molecular volumes V_{calc} of the pristine compounds **1(n)** can be calculated. A comparison with the picnometry data reveals an average difference of only 4 Å^3 (Table 2). This corroborates our WAXD analysis which indicated that a, b, and γ are constant within the odd ($9 \leq n \leq 19$) and even ($12 \leq n \leq 18$) series. Moreover, the anomalous behavior of **1(10)** (20 Å^3) shows the difference between bulk pristine material (WAXD) and the single X-ray crystals obtained from CH$_2$Cl$_2$/THF solution (vide supra).

Summary

Although the electron affinity of 2,5-di-n-alkoxy-1,4-benzoquinones **1(n)** is reduced by the merocyanine-type distortion of 1,4-benzoquinone skeleton, the solid-state intersheet organization of the 1,4-benzoquinone units is considerably improved due to 2,5-di-n-alkoxy substitution. A combination of DSC measurements, density determinations, single-crystal X-ray analyses, and powder WAXD measurements reveal that in the solid state **1(n)** assemble in two-dimensional molecular layers in which the 1,4-benzoquinone moieties stack columnar along both the a and b crystal axes due to an intricate interplay of weak directional hydrogen carbonyl contacts, dipole–dipole interactions, and the hydrophobic ordering effect of the alkyl chain.

DSC measurements show relatively higher melting and solid–solid phase transition temperatures for **1(n)** with short alkyl ($n = 2$, 3, and 4), and in accordance these compounds possess relatively higher densities. The higher analogues ($5 \leq n \leq 19$) display a pronounced odd–even effect in T_{s1} and ΔH_m, and the higher values in the case of $n =$ odd are associated again with relatively higher densities. Since linear relations exist for both enthalpy and entropy changes from a specific alkyl chain length, identical packing structures are expected in the odd ($9 \leq n \leq 19$) as well as even series ($12 \leq n \leq 18$). Large similarities in the powder WAXD patterns in both series support this conclusion. For the pristine **1(n)** the thermal mobility increases markedly at the distinct solid–solid phase transitions (**s2**, $\gamma \rightarrow \beta$: $\Delta S_{s2} = 25\%$ of ΔS_{total} [=conformational entropy], **s1**, $\beta \rightarrow \alpha$: $\Delta S_{s1} = 32\%$ of ΔS_{total}). The considerable degree of conformational freedom in the α-phase (57%) is indicative for the presence of attractive forces between the 1,4-benzoquinone moieties preventing **1(n)** from melting. The irreversibility of the γ-phase in the DSC measurements shows the different behavior of **1(n)** in crystallization from solution and the molten state. Upon crystallization from solution the close packing of the alkyl chains dominates, whereas from the molten state stable packing of the 1,4-benzoquinone moieties prevents a triclinic-like alkoxy chain packing in going from the β- to γ-phase.

The single-crystal X-ray structures of **1(3)**, **1(9)**, and **1(10)** have very similar solid state architectures. Short H···O=C contacts lead to the formation of "one-dimensional" ribbons. Reduction of dipole–dipole interactions and the hydrophobic ordering of alkoxy chains lead to two-dimensional molecular layers from these ribbons. The linear relationships found between the WAXD long-spacing distance ($1/|c^*|$) and n for the entire series ($n = 1-19$) demonstrate the two-dimensional layered structure. Compound **1(3)** displays gauche kinks at the end of the alkoxy chains, which are necessary to obtain a close-packing structure within these layers. In contrast to **1(3)**, the alkoxy chains of **1(9)** and **1(10)** possess an antiperiplanar conformation. Noteworthy is the identical torque present in the alkyl chains, starting at the ether linkage and ending at about an alkoxy chain length of ca. 9 carbon atoms, which is necessary to overcome the incommensurability of the rigid 1,4-benzoquinone moiety and the alkoxy chains. The observed odd–even differences of **1(n)** are, in contrast to n-paraffins, a result of only different alkoxy chain end-group packing. Accurate comparison of the packing motifs of **1(9)** and **1(10)** shows that due to differences in molecular symmetry a looser end-group packing is observed in the even series leading to less ideal thermal behavior.

CM950526W

(58) Stout, G. H.; Jensen, L. H. *X-ray Structure Determination*, 2nd ed.; The Macmillan Company: London, 1969; p 31.